Morphology of Polyethylene with Regular Side Chains Distribution

MIROSLAV JANICEK[*1], ROMAN CERMAK[1,3], PETR PONIZIL[2,3]
[1] Department of Polymer Engineering
[2] Department of Physics and Materials Engineering
Tomas Bata University in Zlín
Namesti T. G. Masaryka 275, 76272 Zlín
CZECH REPUBLIC
[*]corresponding author email: mjanicek@ft.utb.cz http://www.ft.utb.cz
[3] Centre of Polymer Systems
Tomas Bata University in Zlín
Namesti T. G. Masaryka 5555, 76001 Zlín
CZECH REPUBLIC

Abstract: Copolymers of ethylene and α-olefins (consisting of 8, 12, 18 or 26 carbons) synthesized with zirconocene catalyst (which provided regular comonomer distribution) were investigated by differential canning calorimetry and X-ray scattering. As indicated from the calorimetry and small-angle X-ray scattering, the ethylene-hexacosene copolymer with comonomer content of 3 mol% may have a second crystallites present. As no other reflections were measured with wide-angle X-ray scattering, the side chains crystallites should have the same dimensions of its crystal lattice as the main chain crystalline structures. Since this side chains crystallization was found only in the ethylene-hexacosene copolymer with higher content of comonomer, a critical concentration of sufficiently long comonomer chains should be reached for this secondary crystallite formation.

Keywords: alpha-olefin copolymer, morphology, crystalline structure, mLLDPE

1 Introduction

Linear low-density polyethylene (LLDPE) is a copolymer of ethylene with small percentage of but-1-ene, hex-1-ene, or oct-1-ene, which represents significant portion of 60 million tons worldwide annual production of polyethylenes (PE) [1]. LLDPE can be produced using both the Ziegler--Natta (ZN) catalysts, resulting in random comonomer distribution in the chain [2], and the metallocene catalysts which provide regular comonomer distribution [3–5]. Although the metallocene catalysts were broadly studied and applied in polymerization of stereoregular polypropylene [5,6], they were also successfully used for copolymerization of LLDPE [4]. Kaminsky et al. [3] showed that cocatalyst system based on zirconocene is very active also for the copolymerization of ethylene with oct--1-ene. Beside this, the zirconocene complex was used to copolymerize dodec-1-ene, octadec-1-ene and hexacos-1-ene with ethylene to copolymers with regular side chains distribution along the main chain; their properties were subject to study elsewhere [3,7–10].

The macroscopic properties of polyolefins strongly depend on the chain structure, and therefore, the quality of PE in both molten and solid state could be tuned by presence of side chains of various lengths and quantities. This dependence is caused by steric hindrances of the side chains what affects primarily the polymer crystallinity [3]. Generally agreed models also suppose that the side chains are incorporated in the amorphous phase and only a small portion of the side chain atoms is located inside crystalline regions, where they create packing errors [7]. On the contrary, Piel et al. [10] suggested that in some cases these short chains, namely those based on rather long comonomers, can crystallize and possibly create separated aggregates.

The present paper directs attention to assess the presence of second crystalline phase using X-ray scattering (both the wide-angle and small-angle setup) and differential scanning calorimetry (DSC).

2 Experimental

2.1 Materials

Copolymers of ethylene with oct-1-ene, dodec-1--ene, octadec-1-ene and hexacos-1-ene as a comonomer were synthesized as outlined elsewhere

[9,10]. They are here denoted according to the comonomer length (the number following the letter "C") and the initial comonomer concentration (mol%) in a polymerization mixture (the number preceding the letter "C"), which fairly corresponds to the 1.5 and 3.0 mol% comonomer concentration in the copolymer. Summary of their previously published characteristics is given in Table 1, where the reference ethylene homopolymer is denoted as L-PE.

2.2 Differential Scanning Calorimetry

The investigation of thermal behavior was done using a Perkin-Elmer Pyris 1 DSC power-compensated instrument. All measurements were initiated by rapid heating (50 K·min^{-1}) from 20 °C to 160 °C. At this temperature the samples were held for 5 min. Afterwards, cooling (-10 K·min^{-1}) was performed down to 20 °C and after 5 min of settling the material was heated (10 K·min^{-1}) back to 160 °C. Values of each enthalpy change (ΔH_m) were gained using the instrument software and they were recalculated using Eq. (1) to estimate crystallinity (x_c) of each material.

$$x_c = \Delta H_m / \Delta H_m^0 \cdot 100 \ [\%] \qquad (1)$$

The heat of fusion of fully crystallized PE (ΔH_m^0 = 290 J·g^{-1}) was taken from the value listed in previous publications [10]. Lamellar thickness (L_c) can be estimated from the melting peak maximum by the Gibbs-Thomson equation (2) and the Flory equation (3), where T_m is a melting temperature, T_m^c is a copolymer melting temperature, X_e is a molar fraction of ethylene comonomer (for homopolymer X_e = 1), T^0_m = 418.6 K is an equilibrium melting temperature of PE, $\Delta H_u = 2.96 \cdot 10^8$ J·m^{-3} is a volumetric heat of fusion, σ_e = 0.09 J·m^{-2} is a basal surface free energy, and R = 8.314 Pa·m^{3}K^{-1}mol^{-1} is a molar gas constant. The relation between X_e and T_m is curve fitting – Eq. (4), published elsewhere [10].

$$T_m = T_m^c \cdot \left(1 - \frac{2\sigma_e}{\Delta H_u L_c}\right) \qquad (2)$$

$$1/T_m^c = 1/T_m^0 - \ln X_e \cdot R/\Delta H_u \qquad (3)$$

$$\ln X_e = 0.331 - 135.5/T_m \qquad (4)$$

2.3 Sample Preparation

All the samples were subjected to recrystallization under controlled thermal conditions with a Perkin-Elmer DSC instrument. The specimens were in a shape of discs of 4 mm in diameter and thickness of approx 1 mm. Heating from 20 °C to 160 °C was done with rate of 50 K·min^{-1}. In the molten state, the materials were held for 5 min before cooling with rate of -1 K·min^{-1} was done. Specimens were cooled down to 20 °C and they were subsequently used for X-ray diffraction directly, while for the scanning electron microscopy (SEM) the surface was additionally treated by chemical etching in 1 wt% solution of $KMnO_4$ in H_2SO_4 for 15 min. After washing in running water, specimens were washed in acetone and sputter-coated with Pd/Au alloy.

2.4 X-Ray Scattering

Small-angle X-ray scattering (SAXS) was done with Molecular Metrology SAXS System with a pinhole camera attached to a microfocused X-ray beam generator (Osmic MicroMax-002) operating at 45 kV and 0.66 mA. The camera was equipped with a multiwire gas-filled area detector with an active area diameter of 20 cm (Gabriel design).

A Bruker D8 Discover was used to measure wide- angle X-ray scattering (WAXS) which was equipped with X-ray tube with a copper target operating at 30 kV and 30 mA and a GADDS 2-D detector. Mathematical functions were used for fitting of individual intensity vs. 2θ curves using

Table 1. Ethylene copolymers characteristics and branching information calculated by Piel et al. [10]

	M_w	MWD	Conversion[a]	DSC			NMR	
	[kg·mol^{-1}]		[%]	T_m [°C]	T_c [°C]	x_c [%]	MSL[b] (bonds)	MSL[b] [Å]
L-PE	368	2.13	N/A	139.0	115.6	65.6	N/A	N/A
15C8	321	2.19	10.1	115.2	100.6	41.3	120	151.2
15C12	316	2.05	8.8	116.5	100.2	40.5	128	161.3
15C18	328	2.08	8.8	116.5	102.9	41.3	134	168.8
15C26	352	2.22	7.1	118.7	99.7	42.9	140	176.4
30C8	269	2.02	8.8	103.3	85.4	31.3	55	69.3
30C12	280	1.94	7.3	103.3	86.1	31.1	47	59.2
30C18	276	1.98	9.8	104.1	86.9	30.0	50	63.0
30C26	334	2.00	7.7	103.3	85.9	40.2	49	61.7

a) Portion of the initial comonomer content incorporated into the macromolecule.

b) Methylene sequence length – distance between branching carbons. $\mathrm{MSL}[\text{Å}] = (\mathrm{MSL}[\mathrm{bonds}] \cdot 2.52)/2$.

TOPAS software to describe the amorphous and crystalline curves. The crystallinity index (X_c) was subsequently calculated from Eq. (5), where I_c and I_a are intensities of crystalline and amorphous phase, expressed by the area under WAXS curves.

$$X_c = I_c / (I_c + I_a) \cdot 100 \ [\%] \qquad (5)$$

2.5 Scanning Electron Microscopy

A FEI Quanta FEG scanning electron microscope was used for the observation of the etched specimen surfaces; the Everhart-Thornley detector and 5 kV accelerated voltage were employed.

3 Results and Discussion

3.1 Differential Scanning Calorimetry

Table 2 summarizes crystallinity values obtained from Eq. (1). It is clear that the temperatures of transitions of the L-PE are the highest as compared to the rest of the samples (copolymers). This indicates better evolution of ordered structures in L-PE which is also confirmed by its highest x_c. Calculating from the heat of crystallization only slight variation of the crystallinity can be seen in 15C8, 15C12, 15C18 and 15C26. In the set of samples with higher content of side chains the 30C8 shows the highest x_c. The other samples display nearly identical values. Calculating from the heat of fusion the x_c shows similar dependence for the copolymers with lower content of side chains. But for the copolymers with more side chains the values non-monotonically varies.

As expected, the crystallinity indexes and melting/crystallization temperatures for the copolymers with higher content of side chains are always below those with lower side chains content.

In the DSC record no second peak could be observed for any sample except 30C26. This peak at T_m = 49 °C represents heat of 6 J·g^{-1}. It is worth noting that the pure hexacosene wax shows two melting peaks – at 37.3 °C and 52.6 °C, and the investigated copolymer was purified by repeated recrystallization to eliminate any erroneous signals [10]. As a consequence, the revealed peak should be ascribed to the polymer transition.

3.2 Wide-Angle X-Ray Scattering

Table 3 shows the peak positions of the (110) and (200) reflections of all samples. It can be seen, the position of these maxima in case of L-PE is above all the values obtained for the copolymers. This implies that the distance between reflection planes is smaller (according to Bragg's law) when compared to other samples. As mentioned before, we cannot assume that all the side chains will be excluded from the crystalline regions and also Stadler et al. [11] admit the presence of side chains inside the crystallites, which widens the crystal lattice. On the other hand, they suppose that the short side chains will be most likely presented in the lattice in comparison with longer side chains, which remain outside the crystalline regions. These chains are then concentrated on the boundary of crystallites.

Comparing copolymers with different comonomer amount – 15C8 with 30C8 etc., one can see that both the 2θ angle and the X_c are smaller for the samples with higher side chains content than the corresponding values for the samples with low number of side chains, which is in accordance with DSC data. The crystallinity index increases with the increasing comonomer length for both sets of samples. Unfortunatelly, the WAXS determined crystallinities are different from those calculated from the DSC as can arise from recrystallization effect during DSC measurement. In further text, the values mostly from X-ray scattering will be discussed.

Table 2. Recorded and evaluated DSC data.

	crystallization			**melting**			L_c **[Å]**
	T_c **[°C]**	ΔH_c **[J·g^{-1}]**	x_c **[%]**	T_m **[°C]**	ΔH_m **[J·g^{-1}]**	x_c **[%]**	
L-PE	116.0	157.9	54.4	135.0	170.6	58.8	241.3
15C8	99.6	71.4	24.6	113.2	86.4	29.8	78.7
15C12	100.3	76.8	26.5	113.2	90.2	31.1	78.7
15C18	102.1	83.0	28.6	114.2	91.3	31.5	81.2
15C26	100.4	75.3	26.0	115.0	76.4	26.3	83.3
30C8	85.3	72.5	25.0	99.7	58.4	20.1	55.5
30C12	86.1	56.5	19.5	100.5	65.1	22.4	56.5
30C18	85.7	58.3	20.1	102.6	54.7	18.9	59.3
30C26 major peak	85.9	54.6	18.8	101.0	58.0	20.0	57.2
30C26 minor peak	—	—	—	49.0	6.0	—	26.3

3.3 Small-Angle X-Ray Scattering

Fig. 1 shows Lorentz-corrected intensity vs. scattering vector spectra. Expectably, the intensity maximum of the L-PE points the lowest scattering vector (q) of all measured samples, what refers to the biggest long period (LP), i.e. well-developed crystalline structure. The relation between q and LP is determined by Bragg's law – Eq. (6).

$$LP = 2\pi n/q \qquad (6)$$

Combining the WAXS and SAXS data – Eq. (7) and (8), the thicknesses of lamella (l_c) and amorphous layer (l_a) can be estimated [12].

$$l_c = X_c/100 \cdot LP \qquad (7)$$

$$LP = l_c + l_a \qquad (8)$$

3.4 Model

Fig. 2 gives summary of values of methylene sequence length (MSL) derived from nuclear magnetic resonance (NMR) data by Piel et al. [10] compared to L_c, l_c and l_a established in this paper. From the comparison of L_c and l_c with MSL it is evident that the MSL values are higher than L_c or l_c for the low-comonomer materials, and that the MSLs are similar to L_c or l_c for the materials with higher comonomer content. This can be explained by entanglements restricting whole regular methylene sequences to be incorporated into lamellae within melt crystallization; also the maximum lamellar thickness thermodynamically achievable at given crystallization conditions should be considered. It should be also mentioned that the length of the crystallizing sequences (MSL) for the copolymer with 1.5 mol% of comonomer is less than one time higher as compared to the relevant l_c; as for the copolymers with higher comonomer content the values are similar. Even for the copolymer with lower comonomer content the length of crystallizing sequence does not allow to create two consecutive stems during lamellae formation. In both cases the lamellae should not be thus created via regular chain folding but rather a switchboard model approach.

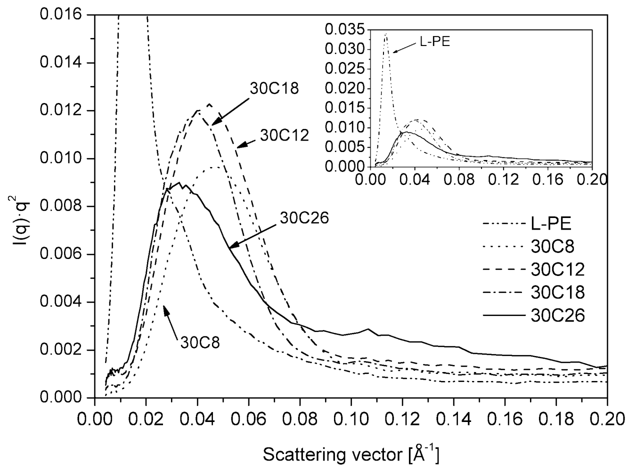

Fig. 1. Lorentz-corrected SAXS patterns

The l_c calculated from the X-ray data for the 30C26 sample is significantly higher than the others in the set of copolymers with 3.0 mol% of comonomer. This phenomenon could be explained that the calculated thickness of the main chain lamellae is increased by the thickness of the lamellae created by the side chains. The maximal lamellar thickness of side-chains lamella is length of straightened chain (30 Å). Regarding the DSC data, the 2nd peak in thermogram of 30C26 points L_c of 26.3 Å, which is in accordance with previously stated. If this length is subtracted from the calculated length of 88 Å, the overestimation is eliminated and the value fits with the others in the set.

Regarding the SAXS patterns, the peak of 30C26 is asymmetrical. Thus the deconvolution into two peaks was done by means of iterative method. The positions of the individual peaks then pointed LP of 194 Å and 122 Å, which means l_c equal to 89 Å and 56 Å. This implies that in some cases the side chains can crystallize in the way that their thickness is added to the thickness of main chain lamellae.

Table 3. Data obtained from WAXS and SAXS measurements and calculated material characteristics.

	Peak position – 2θ [deg]		X_c	q_{max}	LP	l_c	l_a
	(110)	(200)	[%]	[Å^{-1}]	[Å]	[Å]	[Å]
L-PE	21.537	23.906	73	0.01357	463	338	125
15C8	21.432	23.715	48	0.03690	170	82	88
15C12	21.432	23.715	48	0.03551	177	85	92
15C18	21.432	23.732	51	0.03288	191	97	94
15C26	21.415	23.732	55	0.03288	191	104	87
30C8	21.327	23.593	35	0.04648	135	47	88
30C12	21.310	23.575	36	0.04472	141	51	90
30C18	21.310	23.523	40	0.03985	158	63	95
30C26	21.362	23.506	46	0.03288	191	88	103

ISBN: 978-1-61804-022-0

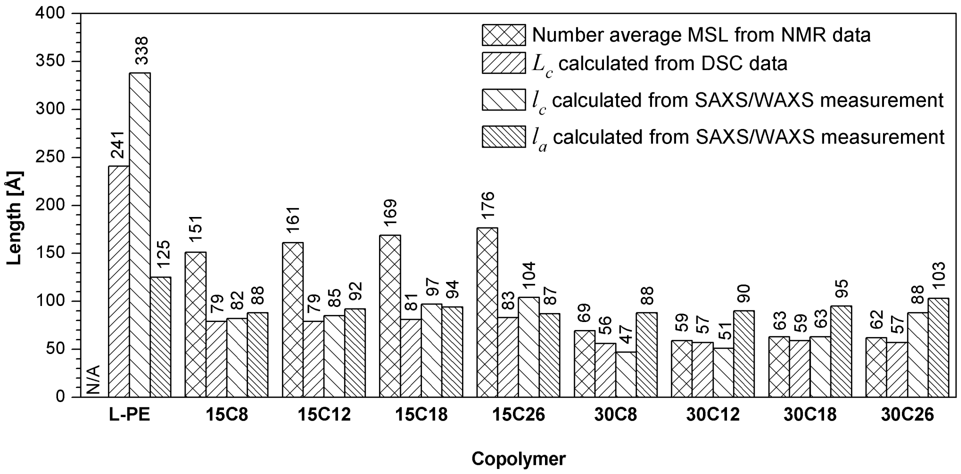

Fig. 2. Comparison of number average MSL (from NMR [10]) with L_c (from DSC), l_c and l_a (from X-ray).

A model comprising two structures of crystalline regions could be proposed. In the material, there should be regions with crystallites created solely by main chain lamellae while the side chains are in an amorphous stay and regions where the side chains are creating crystallites on the surface of main-chain lamellae. An idealized model is given in Fig. 3. As no other diffraction peaks are seen in the WAXS record, we suppose the side chains crystallize in the same crystal lattice dimensions as the main chain.

Because the second crystallites were proved only within the 30C26 sample, two main criteria for their formation can be stated: the sufficient length is necessary to form initial nuclei while the concentration is needed both to have enough of chains to crystallize and to have enough of crystallites to get a signal of detectable intensity. Both seem to be fulfilled only in case of 30C26 copolymer.

It is obvious that the values of MSL and L_c are similar for the materials with 3 mol% of a given comonomer. This implies that the side chains can be in higher concentration localized close to the vicinity of the primary lamellae. The switchboard model of the primary lamellae organization should be here considered based on the mentioned agreement MSL~l_c. Consequently, a strict spatial localization

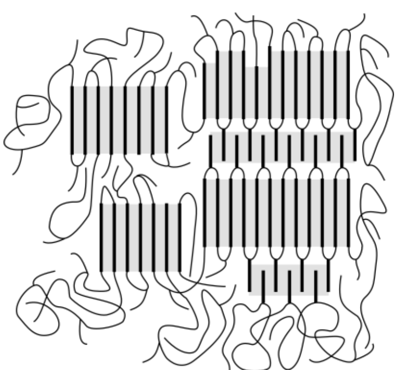

Fig. 3. Idealized model of the crystalline structure.

of the side chains can be supportive to their interaction and nucleation, and overall crystallization.

It should be pointed out that all previous discussion can only be considered if the materials crystallize into the lamellar morphology. To verify this point, SEM was employed showing clearly the formation of lamellar textures (Fig. 4). Unfortunately, in comparison with the SAXS data, the lamellae are thicker as might be related to the effects arising from the etching or metal sputtering. The SEM analysis is therefore used here in terms of qualitative assessment only. One can see that unlike the L-PE the copolymers tend to form spherulites consisting of twisted lamellae.

4 Conclusion

The morphology of metallocene-catalyzed copolymers of ethylene and different α-olefins as a comonomer was studied. The aim was to prove if the side chains are able to crystallize separately to the main chain crystallites. DSC measurements gave evidence of secondary crystalline structures for the hexacosene copolymer with high comonomer content, while the WAXS pattern pointed out, that these structures should have the same crystal lattice size as the prevailing crystallites. Data derived from the X-ray diffraction indicated the second crystalline structures in a size expectable for the side chains lamellae. As the evidence was given only for the hexacosene copolymer with high comonomer content, two main criteria driving the potential side chain crystals formation are discussed: the side chain length and their number should be high enough to let crystallization initiate and proceed. Sufficient amount of the side chains and its specific localization close to the primary lamellae is needed both to have enough crystallizable material and to create enough of crystallites to detect them.

ISBN: 978-1-61804-022-0

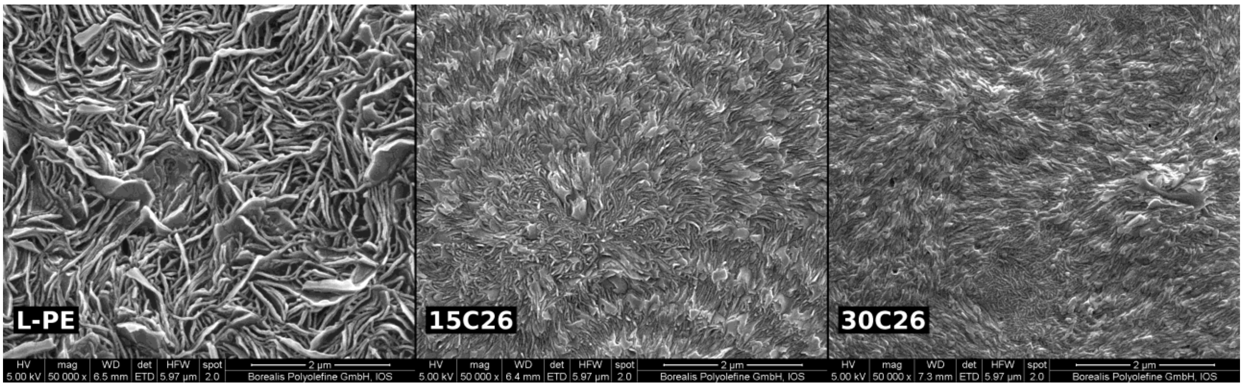

Fig. 4. SEM pictures of the homopolymer and hexacosene copolymers

5 Acknowledgement

We thank to Dr. Martin Obadal for fruitful discussions, to Dr. Christian Piel for the copolymers provision, to Dr. Senthil K. Kaliappan for WAXS measurements and to Dr. Gottfried Kandioller for SEM pictures; all mentioned are of Borealis Polyolefine GmbH.

The work was supported by the Operational Programme Research and Development for Innovations co-funded by the European Regional Development Fund (ERDF) and national budget of Czech Republic within the framework of the Centre of Polymer Systems project (reg. number: CZ.1.05/2.1.00/03.0111).

Author Miroslav Janicek gratefully acknowledges the financial support of this work by the internal grant of TBU in Zlin, No. IGA/11/FT/11/D funded from the resources of specific university research.

References:

[1] Rojas G. *et al.* Precision polyolefin structure: Modeling polyethylene containing alkyl branches, *Polymer*, 49, 13–14, 2008, pp. 2985–2995.

[2] Hernandez R. J. Plastics in packaging. *In* Handbook of plastics, Elastomers & Composites; Harper, C. A., Ed.; McGraw-Hill Professional: New York, 2002.

[3] Kaminsky W. *et al.* Tailoring polyolefins by metallocene catalysis: kinetic and mechanistic aspects, *Journal of Molecular Catalysis A: Chemical*, 213, 1, 2004, pp. 15–19.

[4] Kaminsky W. New polymers by metallocene catalysis, *Macromolecular Chemistry and Physic*, 197, 12, 1996, pp. 3907–3945.

[5] Kaminsky W. Zirconocene catalysts for olefin polymerization, *Catalysis Today*, 20, 2, 1994, pp. 257–271.

[6] Razavi A. *et al.* Site selective ligand modification and tactic variation in polypropylene chains produced with metallocene catalysts, *Coordination Chemistry Reviews*, 250, 1-2, 2006, pp. 155–169.

[7] Stadler F. J. *et al.* Lattice sizes, crystallinities, and spacing between amorphous chains – characterization of ethene-/alpha-olefin copolymers with various comonomers and comonomer contents measured by wide angle X-ray scattering, *e-Polymers*, no.40, 2009.

[8] Stadler F. J. *et al.* Influence of type and content of various comonomers on long-chain branching of ethene/alpha-olefin copolymers, *Macromolecules*, 39, 4, 2006, pp. 1474–1482.

[9] Piel C. *et al.* Structure-property relationships of linear and long-chain branched metallocene high-density polyethylenes and SEC-MALLS, *Macromolecular Chemistry and Physic*, 207, 1, 2006, pp. 26–38.

[10] Piel C. *et al.* Thermal and mechanical analysis of metallocene-catalyzed ethene-alpha-olefin copolymers: The influence of the length and number of the crystallizing side chains, *Journal of Polymer Science Part A-Polymer Chemistry*, 44, 5, 2006, pp. 1600–1612.

[11] Stadler F. J. *et al.* Crystallite dimensions – characterization of ethene-α-olefin copolymers with varios comonomers and comoner contents measured by small- and wide angle X-ray scattering, *e-Polymers*, no.41, 2009.

[12] Roe, R.J. Methods of X-ray and neutron scattering in polymer science. *In* Topics in polymer science; Mark, J.E., Ed.; Oxford University Press: New York, 2000.